HEAT TRANSFER
Asian Research

WILEY

Check for
updates

ORIGINAL ARTICLE

Soret effects on the mixed convection flow using Robin boundary conditions

Jawali C. Umavathi[1] | **Mikhail A. Sheremet[2]** | **Sapnali Limbraj Patil[3]**

[1]Dipartimento di Ingegneria, Università degli Studi della Campania "Luigi Vanvitelli", Aversa, Italy

[2]Laboratory on Convective Heat and Mass Transfer, Tomsk State University, Tomsk, Russia

[3]Department of Mathematics, Gulbarga University, Gulbarga, Karnataka, India

Correspondence
Mikhail A. Sheremet, Laboratory on Convective Heat and Mass Transfer, Tomsk State University, 36 Lenin Avenue, Tomsk, 634050 Russia.
Email: Michael-sher@yandex.ru

Abstract

An investigation has been undertaken as Soret and Schmidt outcomes on the mixed convection flow using Robin boundary conditions. The results use a vertical channel being kept at constant cold temperature and concentration at the left wall and hot temperature and concentration at the right wall. The exchange of heat is done by help of plates with a fluid. We consider the external fluid with equal and different temperatures. This physical problem is solved by using nondimensional parameters with the corresponding boundary conditions. To find analytical solution, the regular perturbation series method is used, and for finding the numerical solution, the well-known Runge–Kutta method with shooting technique is employed. Comparison of the current study is favorable with the previous published results. The obtained results depend on the governing parameters such as thermal Grashof number, solutal Grashof number, Biot numbers, symmetric and asymmetric wall temperatures, Schmidt number, Soret number, and Brinkman number. An influence of these parameters on the fields of velocity, temperature, and concentration is reported. Further, the numerical results for the Nusselt number, mean value of the velocity, dimensionless bulk temperature, skin friction, and molecular diffusion coefficient are tabulated for different parametric conditions and explained. For small

value of Brinkman number, the obtained values agree with other published results for all considered cases.

1 | INTRODUCTION

The induced buoyancy flows in ducts deserve wide attention in the engineering section owing to their usefulness in a huge number of thermally controlled devices such as the heat exchangers, electronics, solar collectors, and others. In the passive- or semipassive-controlled systems, purely free and mixed convection is done. Both the natural and forced convection heat transfer mechanisms take place in the heat transfer situations and that phenomenon is called mixed convection. The internal flow of fluid is either upward or downward in the vertical channels. The flow of mixed convection in vertically heated channels happens in various technical apparatus including internal cooling system by turbine rotor blade and cooling of the nuclear reactors and electronic components. Tao[1] worked on using the vertical channels flow of fully developed mixed convection at the wall temperature. Aung and Worku[2,3] studied the flow of fluid through the vertical channel by the theory of combined free and forced convention and they also assumed that temperature is asymmetric at the walls of the channel. Aung and Worku,[3] Barletta,[4] and Umavathi et al[5] worked on the mixed convection flow of fluid at symmetric wall conditions in vertical channels. Later, Prathap Kumar et al[6-9] studied mixed convection flows in a vertical channel filled with immiscible fluids.

Recently, in the presence of chemical reaction, the coupled heat and mass transfer has many processes. Distribution of temperature and moisture in agricultural field in drying processes, water body evaporation, fruit tree growing, freezing on crops, the energy transfer in the wet cooling tower, etc characterize a simultaneously transfer of heat and mass. In many industries, this type of flow can be observed. By the moving conducting fluid, the electrical energy is extracted in the power industry using the method as generating electric power. By the homogeneous and heterogeneous processes, the chemical reactions are modeled. That depends on an interface or a single-phase volume reaction. In a given phase, the one and only one homogeneous reaction occurs uniformly. Following the work of Das et al,[10] Muthucumarswamy and Ganesan[11] and Prathap Kumar et al[12,13] worked on the effect of first-order chemical reaction on mixed convection flow of multifluid in vertical channel. Umavathi and Jaweriya[14] analyzed the concentration effects on mixed convective flow of a micropolar fluid in a vertical duct. Umavathi and Syed[15] studied the influence of thermophysical variable properties on liquid circulation in a duct using the first-order chemical reaction.

In the case of chemical engineering and industrial section, the transfer of mass and the multicomponent fluid is involved from point to point. By the concentration and temperature gradient, energy flux is generated. The Dufour effect is energy flux obtained by the concentration variation and the Soret effect is the mass flux generated by the temperature gradient. When the temperature and concentration gradients are high, the mentioned effects are very significant. Li et al[16] studied, using the implicit finite volume method, the strong endothermic chemical reacting flow in a porous medium effected by Soret and Dufour phenomena. They found that the Soret and Dufour influences are very

strong for high initial temperature and very low conventional velocity of the feeding gas. Sheremet[17] investigated, numerically, double-diffusive natural convection in a cavity with solid walls and local energy and contaminant sources under the impacts of Soret and Dufour phenomena. It was observed that a growth of the Soret parameter characterizes a rise of the average Nusselt number at the heat source and a reduction of the mass transfer coefficient at the contaminant source.

Following the works of Kandasamy et al,[18,19] Seddeek[20] worked on the chemical reaction by heat and mass transfer and on magnetohydrodynamics (MHD) free convective heat generation by thermal radiation and by buoyancy effects. After this, Seddeek and co-workers[21-23] pointed out the MHD convection flow along the chemical reaction, variable viscosity, and thermal radiation. Chamkha and Ben-Nakhi[24] studied MHD flow along vertical permeable surface in porous medium with the presence of Soret and Dufour effect, while Pal and Mondal[25] and Shivaiah and Rao[26] studied the non-Darcy unsteady MHD mixed convection with heat and mass transfer in the presence of Soret and Dufour effects. Zheng et al[27] and Cheng[28] worked on the Soret and Dufour effects on MHD flow and mixed convection with constant wall temperature and concentration. Also, Devi and Devi[29] studied the Soret and Dufour influences on magnetic slip motion combined with thermal radiation over a porous rotating disk. Rashad and Chamkha[30] pointed out the porous media natural convection flow through the heat and mass transfer with effects of Soret and Dufour. Shivaiah and Rao,[31] and Makinde[32] investigated unsteady MHD convection with the influences of Soret, Dufour, thermal radiation, and chemical reaction. Rashidi et al[33] discussed the viscous, laminar mixed convection boundary layer flow over a horizontal plate with chemical reaction. A very new concept of group theory was employed to determine the invariant solutions of the conservation equations. Recently, Sarwar and Rashidi[34] investigated the analytical approximate solutions for the Caputo-type fractional-order two-term diffusion, wave-diffusion, and telegraph equations. Homotopy method was used by Rashidi et al[35] and Hany and Rashidi[36] to study the axisymmetric unsteady two-dimensional flow of nonconducting, incompressible second grade fluid between two circular plates and for the micropolar flow in a porous channel with mass injection for different values of Reynolds number, respectively. It is interesting to note that Rashidi et al[37] were also successful in employing the homotopy perturbation method to solve the nonlinear time function for the equations of motion based on the Von-Karman theory for a rectangular isotropic plate considering the effect of shear deformation and rotary inertia. Makinde and Olanrewaju[38] worked on the effects of Soret and Dufour on analyzed unstudied mixed convection.

Wibulswal,[39] Lyczkowski et al,[40] and Javeri[41] expressed the thermal entrance region of a rectangular channel with the convective energy transport under laminar mode for the first kind of thermal boundary condition, while Hicken[42] and Sparrow and Siegel[43] studied the boundary condition of the second kind, expressed by the prescribed wall heat flux.

Javeri[44] worked on the boundary condition of third kind for heat transfer in laminar regime. Also, Javeri[45] explored the energy transport in a rectangular channel under the third kind of thermal boundary condition at the wall. Later, Zanchini[46] analyzed the vertical channel mixed convection flow with the boundary condition of third kind.

In the present study, the authors analyzed the viscous fluid flow, heat and mass transfer characteristics through the vertical channel employing the boundary conditions of third kind. These results can be applicable in many industries, transportation network, biomedical section, and in electronics branches.

2 | MATHEMATICAL FORMULATION

Here we contemplate the laminar flow in the parallel plate vertical channel with incompressible fluid. The X-axis lies on the axial plane and it shows direction of gravity. The Y-axis lies along the perpendicular to the walls. The vertical channel occupies the region $-L/2 \leq Y \leq L/2$, which is shown in Figure 1. The flow is fully developed, steady-state, and incompressible. The flow is driven by buoyancy due to temperature and concentration gradients in a vertical channel. Viscous heating is also included in the model. Thermal dispersion, cross-diffusion, and stratification effects are neglected. In addition, the concentration of the solute constituent in the solution at the left wall is C_1 and at the right wall is C_2, in a way, such that $C_2 \geq C_1$. An (X, Y) co-ordinate system is employed and the origin is located at the mid-plane of the channel. The channel walls are infinite in the X-direction. Therefore the flow becomes one-dimensional along the X-axis, and hence velocity is a function of Y-co-ordinate only. The thermal conductivity, thermal diffusivity, dynamic viscosity, and thermal expansion coefficient of fluids are considered to be fixed. The Boussinesq approximation is stated as

$$\rho = \rho_0 [\beta_T (T - T_0) - \beta_C (C - C_0)]. \tag{1}$$

Again, considering the equations of continuity with $\nabla \cdot U = 0$, gives

$$\frac{\partial U}{\partial X} = 0. \tag{2}$$

Component U depends only on Y-co-ordinate. Then considering the balance equation for X-axis and for Y-axis, following can be obtained (following Zanchini,[46] Umavathi et al,[14,15] and Muthucumaraswamy and Ganesan[11])

$$\beta_T g (T - T_0) + \beta_C g (C - C_0) - \frac{1}{\rho_0} \frac{\partial P}{\partial X} + \nu \frac{d^2 U}{dY^2} = 0, \tag{3}$$

$\bar{g}$

X

Y

$T = T_1$
$C = C_1$
$Y = -0.5L$

$T = T_2$
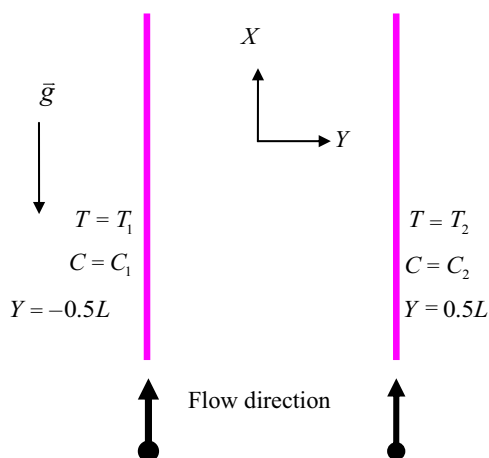$C = C_2$
$Y = 0.5L$

Flow direction

FIGURE 1   Schematic diagram [Color figure can be viewed at wileyonlinelibrary.com]

$$\frac{\partial P}{\partial Y} = 0. \tag{4}$$

As a result, $P = p + \rho_0 g X$. By Equation (4), it is shown that P depends only on X. As a result, Equation (3) can be rewritten as

$$(T - T_0) = \frac{1}{\rho_0 g \beta_T} \frac{dP}{dX} - \frac{\mu}{\rho_0 g \beta_T} \frac{d^2 U}{dY^2} - \frac{\beta_C}{\beta_T} (C - C_0). \tag{5}$$

Equation (5) implies that

$$\frac{\partial T}{\partial X} = \frac{1}{\rho_0 g \beta_T} \frac{d^2 P}{dX^2}, \tag{6}$$

$$\frac{\partial T}{\partial Y} = -\frac{1}{\rho_0 g \beta_T} \frac{d^3 U}{dY^3} - \frac{\beta_C}{\beta_T} \frac{\partial C}{\partial Y}, \tag{7}$$

$$\frac{\partial^2 T}{\partial Y^2} = -\frac{1}{\rho_0 g \beta_T} \frac{d^4 U}{dY^4} - \frac{\beta_C}{\beta_T} \frac{\partial^2 C}{\partial Y^2}. \tag{8}$$

Two walls exchange the heat by convection with external fluid and its thickness is very negligible. At $Y = -L/2$ and $Y = L/2$, we have h_1 and h_2 as the external heat transfer coefficients. The uniform reference temperatures are T_1 and T_2 of the fluid occupying the region $Y < -L/2$ and $Y > L/2$, respectively. The temperature boundary conditions are given as $(T_2 \geq T_1)$

$$-k \frac{\partial T}{\partial Y} \bigg|_{-L/2} = h_1 [T_1 - T(X, -L/2)], \tag{9}$$

$$-k \frac{\partial T}{\partial Y} \bigg|_{L/2} = h_2 [T(X, L/2) - T_2]. \tag{10}$$

Equations (9) and (10) can be rewritten using Equation (7)

$$\frac{d^3 U}{dY^3} \bigg|_{Y=-L/2} = \frac{\beta_T g h_1}{k \upsilon} \left(1 - \frac{k \beta_C}{T \beta_T}\right) [T_1 - T(X, -L/2)], \tag{11}$$

$$\frac{d^3 U}{dY^3} \bigg|_{Y=L/2} = \frac{\beta_T g h_2}{k \upsilon} \left(1 - \frac{k \beta_C}{T \beta_T}\right) [T(X, L/2) - T_2]. \tag{12}$$

Equations (11) and (12) show that $\partial T/\partial X = 0$ at both walls. It shows that the term $\partial T/\partial X$ is independent on Y-co-ordinate. It led to the conclusion that $\partial T/\partial X$ is zero everywhere. Therefore, temperature T depends only on Y; then

$$\frac{dP}{dX} = A, \tag{13}$$

where A is constant. The energy balance equation for viscous dissipation can be stated as:

$$\frac{d^2T}{dY^2} = -\frac{\upsilon}{\alpha C_p}\left(\frac{dU}{dY}\right)^2. \tag{14}$$

The concentration equation is:

$$\frac{d^2C}{dY^2} = -\frac{k}{T}\frac{d^2T}{dY^2}. \tag{15}$$

From Equations (8) and (14), we have another equation for component U

$$\frac{d^4U}{dY^4} = \frac{\beta_T g}{\alpha C_p}\left(\frac{dU}{dY}\right)^2 - \frac{\beta_C gk}{\alpha C_p T}\left(\frac{dU}{dY}\right)^2. \tag{16}$$

Boundary conditions for the velocity are

$$U(-L/2) = 0, \quad U(L/2) = 0. \tag{17}$$

From Equation (5), Equations (11) and (12) can be rewritten as

$$\frac{d^3U}{dY^3}\bigg|_{Y=-L/2} - \frac{h_1}{k}\frac{d^2U}{dY^2}\bigg|_{Y=-L/2} = -\frac{Ah_1}{\mu k} + \frac{\beta_T gh_1}{\upsilon k}[T_1 - T_0] + \frac{\beta_C gh_1}{k\upsilon}[C_1 - C_0], \tag{18}$$

$$\frac{d^3U}{dY^3}\bigg|_{Y=L/2} + \frac{h_2}{k}\frac{d^2U}{dY^2}\bigg|_{Y=L/2} = \frac{Ah_2}{\mu k} + \frac{\beta_T gh_2}{\upsilon k}[T_0 - T_2] + \frac{\beta_C gh_2}{k\upsilon}[C_2 - C_0]. \tag{19}$$

Equation (15) using Equation (14) becomes

$$\frac{d^2C}{dY^2} = \frac{k\upsilon}{T\alpha C_p}\left(\frac{dU}{dY}\right)^2. \tag{20}$$

The boundary conditions on the concentration are

$$C(-L/2) = C_1, \quad C(L/2) = C_2. \tag{21}$$

The dimensionless parameters are

$$u = \frac{U}{U_0}, \quad \theta = \frac{T - T_0}{\Delta T}, \quad y = \frac{Y}{D}, \quad GR_T = \frac{g\beta_T \Delta T D^3}{v^2}, \quad \text{Re} = \frac{U_0 D}{v},$$

$$Br = \frac{U_0^2 \mu}{k\Delta T}, \quad R_T = \frac{T_2 - T_1}{\Delta T}, \quad GR_C = \frac{g\beta_C \Delta T D^3}{v^2}, \quad \Lambda_1 = \frac{GR_T}{\text{Re}}, \quad \Lambda_2 = \frac{GR_C}{\text{Re}},$$

$$Bi_1 = \frac{h_1 D}{k}, \quad Bi_2 = \frac{h_2 D}{k}, \quad S = \frac{Bi_1 Bi_2}{Bi_1 Bi_2 + 2Bi_1 + 2Bi_2}, \quad U_0 = -\frac{AD^2}{48\mu},$$

$$\phi = \frac{C - C_0}{\Delta C}, \quad Sc = \frac{v}{D_m}, \quad Sr = \frac{k \Delta T D_m}{T \Delta C v}.$$

(22)

where $D = 2L$ is the hydraulic diameter, while velocity and temperature references are written as

$$U_0 = -\frac{AD^2}{48\mu}, \quad T_0 = \frac{T_1 + T_2}{2} + S\left(\frac{1}{Bi_1} - \frac{1}{Bi_2}\right)[T_2 - T_1], \quad C_0 = \frac{C_1 + C_2}{2}. \tag{23}$$

The reference temperature field difference is:

$$\Delta T = T_2 - T_1 \ if \ T_1 < T_2, \tag{24}$$

$$\Delta T = \frac{v^2}{C_p D^2} \ if \ T_1 = T_2, \tag{25}$$

$$\Delta C = C_2 - C_1. \tag{26}$$

Therefore, the value of the dimensionless parameter R_T can be either 0 or 1. More precisely, R_T equals 1 for asymmetric fluid temperatures, $T_1 < T_2$, and equals 0 for symmetric fluid temperatures, $T_1 = T_2$. The dimensionless equations can be considered in the following form

$$\frac{d^4 u}{dy^4} = (\Lambda_1 - \Lambda_2 \cdot Sr \cdot Sc) Br \left(\frac{du}{dy}\right)^2 \tag{27}$$

with velocity boundary conditions

$$u(-1/4) = u(1/4) = 0, \tag{28}$$

$$\frac{d^2 u}{dy^2} - \frac{1}{Bi_1} \frac{d^3 u}{dy^3}\bigg|_{y=-1/4} = -48 + \frac{R_T \Lambda_1 S}{2}\left(1 + \frac{4}{Bi_1}\right) + \frac{\Lambda_2}{2}, \tag{29}$$

$$\frac{d^2 u}{dy^2} + \frac{1}{Bi_2} \frac{d^3 u}{dy^3}\bigg|_{y=1/4} = -48 - \frac{R_T \Lambda_1 S}{2}\left(1 + \frac{4}{Bi_2}\right) - \frac{\Lambda_2}{2}, \tag{30}$$

$$\frac{d^2\phi}{dy^2} + Br \cdot Sr \cdot Sc \left(\frac{du}{dy}\right)^2 = 0, \tag{31}$$

$$\phi\left(-\frac{1}{4}\right) = -\frac{1}{2}, \quad \phi\left(\frac{1}{4}\right) = \frac{1}{2}. \tag{32}$$

Similarly, Equations (14) and (22) yield

$$\frac{d^2\theta}{dy^2} + Br \left(\frac{du}{dy}\right)^2 = 0, \tag{33}$$

while from Equations (5) and (22), one obtains

$$\theta = -\frac{1}{\Lambda_1}\left(48 + \frac{d^2u}{dy^2} + \Lambda_2\phi\right). \tag{34}$$

3 | SOLUTIONS

Equations (27) to (32) are highly nonlinear. We resort to approximate analytical solutions using regular perturbation series method, whose solutions are valid for small values of Brinkman number. Assuming Brinkman number to be the perturbation parameter, the solution of Equations (27) to (32) can be written as

$$u(y) = u_0(y) + Br \cdot u_1(y) + Br^2 \cdot u_2(y) + \cdots \tag{35}$$

$$\phi(y) = \phi_0(y) + Br \cdot \phi_1(y) + Br^2 \cdot \phi_2(y) + \cdots \tag{36}$$

Then we got the solutions of Equations (27) to (30) using Equations (35) and (36) and equating the like powers of Br, which leads to a sequence of the unknown function $u_n(y)$ as follows.

3.1 | Solution to Zeroth-order BVP

Equating the zero power coefficient of Brinkman number $n = 0$, we obtain

$$\frac{d^4u_0}{dy^4} = 0 \tag{37}$$

and the corresponding boundary conditions are

$$u_0(-1/4) = u_0(1/4) = 0, \tag{38}$$

$$\left.\frac{d^2u_0}{dy^2}\right|_{y=-1/4} - \frac{1}{Bi_1}\left.\frac{d^3u_0}{dy^3}\right|_{y=-1/4} = -48 + \frac{R_T\Lambda_1 S}{2}\left(1 + \frac{4}{Bi_1}\right) + \frac{\Lambda_2}{2}, \tag{39}$$

$$\left. \frac{d^2 u_0}{dy^2} \right|_{y=1/4} + \frac{1}{Bi_2} \left. \frac{d^3 u_0}{dy^3} \right|_{y=1/4} = -48 - \frac{R_T \Lambda_1 S}{2} \left(1 + \frac{4}{Bi_2} \right) - \frac{\Lambda_2}{2}. \tag{40}$$

The solution of Equation (37) using boundary conditions (38) to (40) is given by

$$u_0(y) = -\frac{C_1 y^3}{6} - \frac{C_2 y^2}{2} - C_3 y - C_4. \tag{41}$$

Then solutions for whole series at $n > 0$ are

$$\frac{d^4 u_n}{dy^4} = \sum_{n=0}^{\infty} (\Lambda_1 - \Lambda_2 \cdot Sc \cdot Sr) \frac{du_j}{dy} \frac{du_{n-j-1}}{dy}, \tag{42}$$

with the boundary conditions

$$u_n(-1/4) = u_n(1/4) = 0, \tag{43}$$

$$\left. \frac{d^2 u_n}{dy^2} \right|_{y=-1/4} - \frac{1}{Bi_1} \left. \frac{d^3 u_n}{dy^3} \right|_{y=-1/4} = 0, \tag{44}$$

$$\left. \frac{d^2 u_n}{dy^2} \right|_{y=1/4} + \frac{1}{Bi_2} \left. \frac{d^3 u_n}{dy^3} \right|_{y=1/4} = 0. \tag{45}$$

Then the solution is in Equation (36) from Equation (31) by equating the like powers of Brinkman number. Thus, we obtain the sequence for this problem and yield the function $\phi_n(y)$

$$\frac{d^2 \phi_0}{dy^2} = 0 \tag{46}$$

with the boundary conditions

$$\phi_0 \left(-\frac{1}{4} \right) = -\frac{1}{2}, \quad \phi_0 \left(\frac{1}{4} \right) = \frac{1}{2}. \tag{47}$$

The solution of Equation (46) is given by

$$\phi_0 = C_5 y + C_6 \tag{48}$$

Then the whole recurrence relations for every $n > 0$ is

$$\frac{d^2 \phi_n}{dy^2} = \sum_{n=0}^{\infty} Sc \cdot Sr \cdot \frac{du_j}{dy} \frac{du_{n-j-1}}{dy} \tag{49}$$

with the boundary conditions
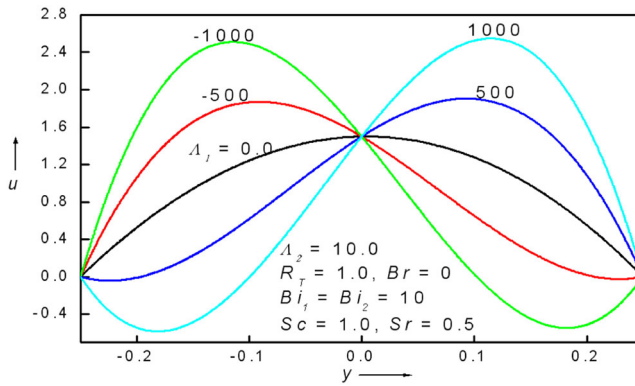
FIGURE 2 Velocity profiles for $\Lambda_1 = -500, -1000, 0.0, 500, 1000$ [Color figure can be viewed at wileyonlinelibrary.com]
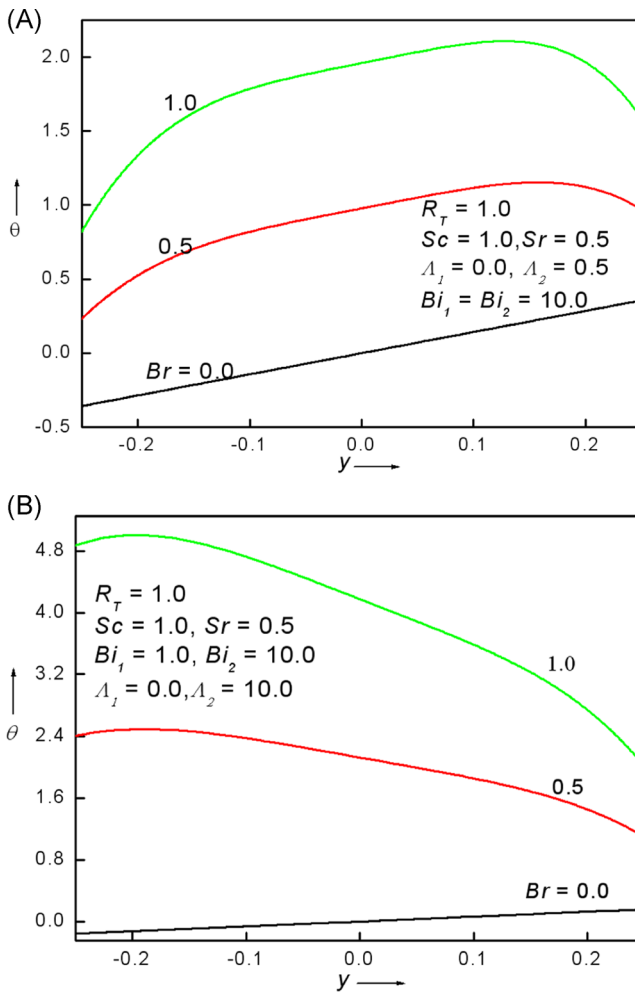
FIGURE 3 A, Temperature profiles for $Br = 0, 0.5, 1.0$. B, Temperature profiles for $Br = 0, 0.5, 1.0$ [Color figure can be viewed at wileyonlinelibrary.com]

$$\phi_n\left(-\frac{1}{4}\right) = \phi_n\left(\frac{1}{4}\right) = 0. \tag{50}$$

From Equation (41), we obtained the function as $u_0(y)$ and the solutions for Equations (42) to (45) are $u_n(y)$, $n > 0$. The solution for θ from Equations (34), (41), and (48) is

$$\theta(y) = 2R_T \cdot S \cdot y - \frac{1}{\Lambda_1}\left[2\Lambda_2 y(1-S) + \frac{\Lambda_2}{2}\left(1 - S\left(1 + \frac{4}{Bi_1}\right)\right) + \sum_{n=1}^{\infty} Br^n\left(\Lambda_2 \phi_n + \frac{d^2 u}{dy^2}\right)\right]. \tag{51}$$

3.2 | Nusselt number, skin friction, and Sherwood number

The definition for Nusselt number is given as follows:

$$Nu_1 = \frac{D}{R_T[T(L/2) - T(-L/2)] + (1-R_T)\Delta T} \frac{dT}{dY}\bigg|_{Y=-L/2}, \tag{52}$$

$$Nu_2 = \frac{D}{R_T[T(L/2) - T(-L/2)] + (1-R_T)\Delta T} \frac{dT}{dY}\bigg|_{Y=L/2}. \tag{53}$$
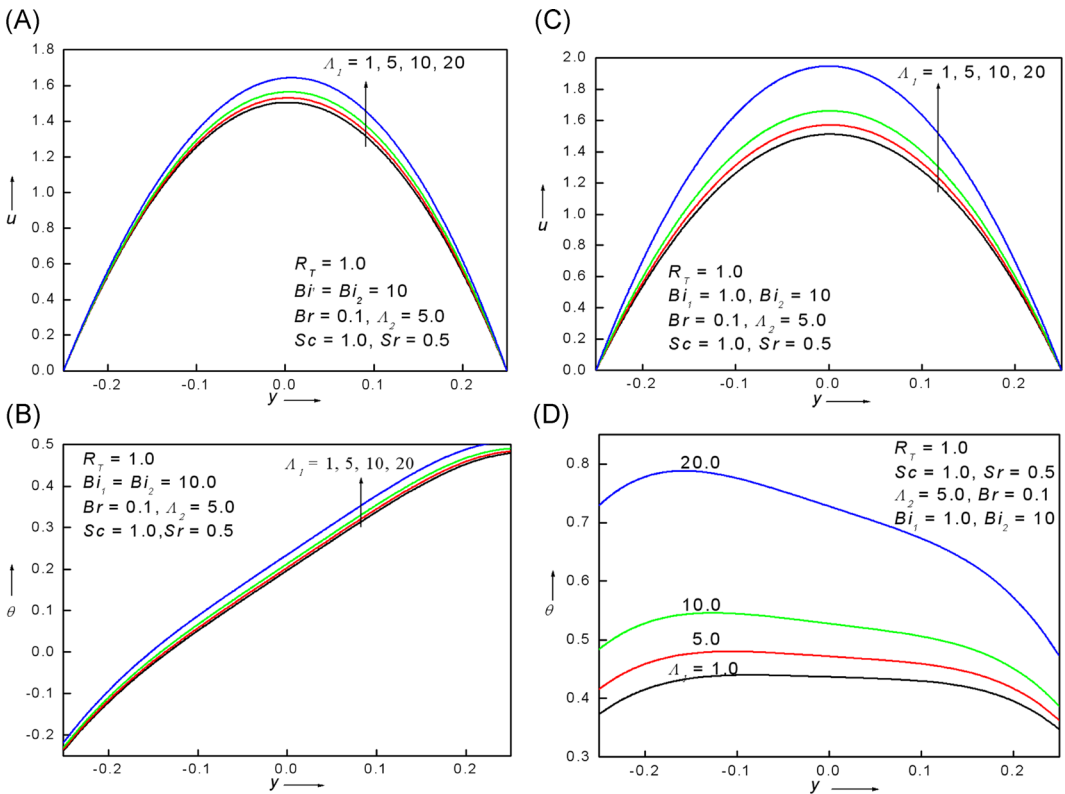
FIGURE 4 A, Velocity profiles for $\Lambda_1 = 1, 5, 10, 20$. B, Temperature profiles for $\Lambda_1 = 1, 5, 10, 20$. C, Velocity profiles for $\Lambda_1 = 1, 5, 10, 20$. D, Temperature profiles for $\Lambda_1 = 1, 5, 10, 20$ [Color figure can be viewed at wileyonlinelibrary.com]

Equations (53) and (52) rewritten using Equation (22) are

$$Nu_1 = \frac{D}{R_T\left[\theta(1/4) - \theta(-1/4)\right] + (1 - R_T)} \frac{d\theta}{dy}\bigg|_{y=-1/4}, \tag{54}$$

$$Nu_2 = \frac{D}{R_T\left[\theta(1/4) - \theta(-1/4)\right] + (1 - R_T)} \frac{d\theta}{dy}\bigg|_{y=1/4}. \tag{55}$$

Similarly, skin friction and Sherwood numbers in dimensionless form become:

$$\tau_1 = \left(\frac{du}{dy}\right)_{y=-\frac{1}{4}}, \quad \tau_2 = \left(\frac{du}{dy}\right)_{y=\frac{1}{4}} \tag{56}$$

$$Sh_1 = \left(\frac{d\phi}{dy}\right)_{y=-\frac{1}{4}}, \quad Sh_2 = \left(\frac{d\phi}{dy}\right)_{y=\frac{1}{4}}. \tag{57}$$
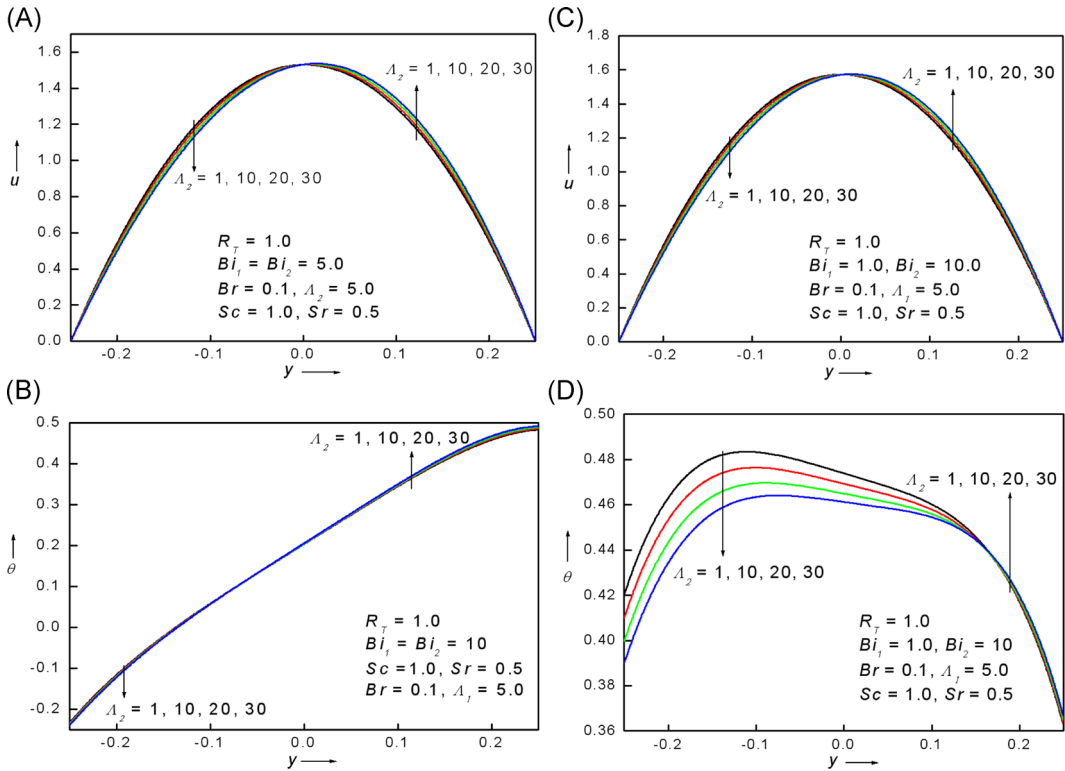
FIGURE 5 A, Velocity profiles for $\Lambda_2 = 1$, 10, 20, 30. B, Temperature profiles for $\Lambda_2 = 1$, 10, 20, 30. C, Velocity profiles for $\Lambda_2 = 1$, 10, 20, 30. D, Temperature profiles for $\Lambda_2 = 1$, 10, 20, 30 [Color figure can be viewed at wileyonlinelibrary.com]

3.3 | Mean velocity and bulk temperature

The average velocity $\bar{u}$ and the bulk temperature θ_b

$$\bar{u} = 2 \int_{-1/4}^{1/4} u \, dy, \tag{58}$$

$$\theta_b = \frac{2}{\bar{u}} \int_{-1/4}^{1/4} u \cdot \theta \, dy. \tag{59}$$
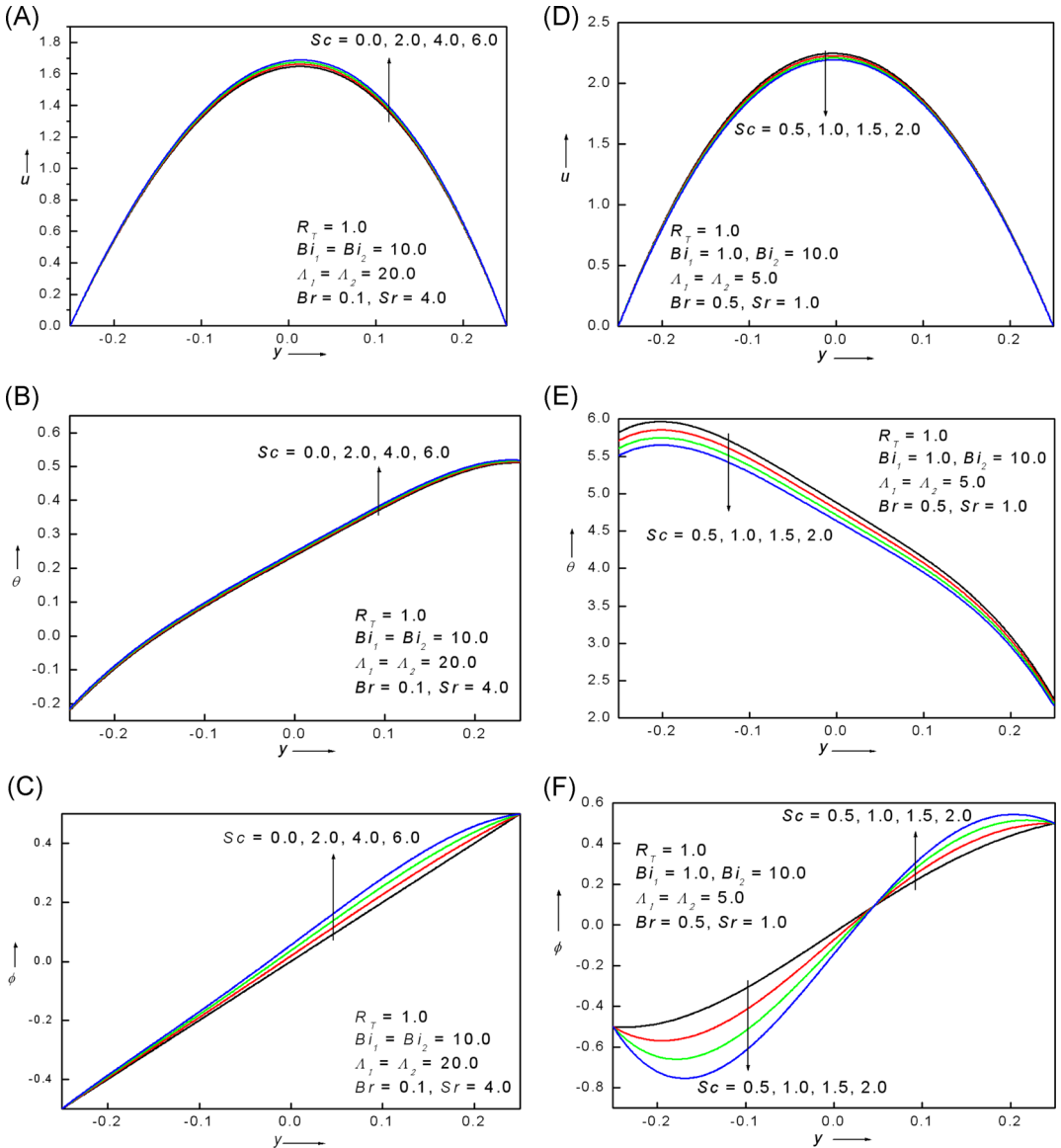
FIGURE 6 A, Velocity profiles for $Sc = 0, 2, 4, 6$. B, Temperature profiles for $Sc = 0, 2, 4, 6$. C, Concentration profiles for $Sc = 0, 2, 4, 6$. D, Velocity profiles for $Sc = 0.5, 1.0, 1.5, 2.0$. E, Temperature profiles for $Sc = 0.5, 1.0, 1.5, 2.0$. F, Concentration profiles for $Sc = 0.5, 1.0, 1.5, 2.0$ [Color figure can be viewed at wileyonlinelibrary.com]

4 | NUMERICAL SOLUTIONS

By the regular perturbation method, all above results are obtained and they are valid for small Brinkman numbers as perturbation parameter. The solution is valid to whole series by using numerical methods as using Runge–Kutta fourth-order integration scheme. Validity of the numerical scheme is justified by comparing the analytical solutions with the numerical solutions and good agreement is found for small values of the perturbation parameter.
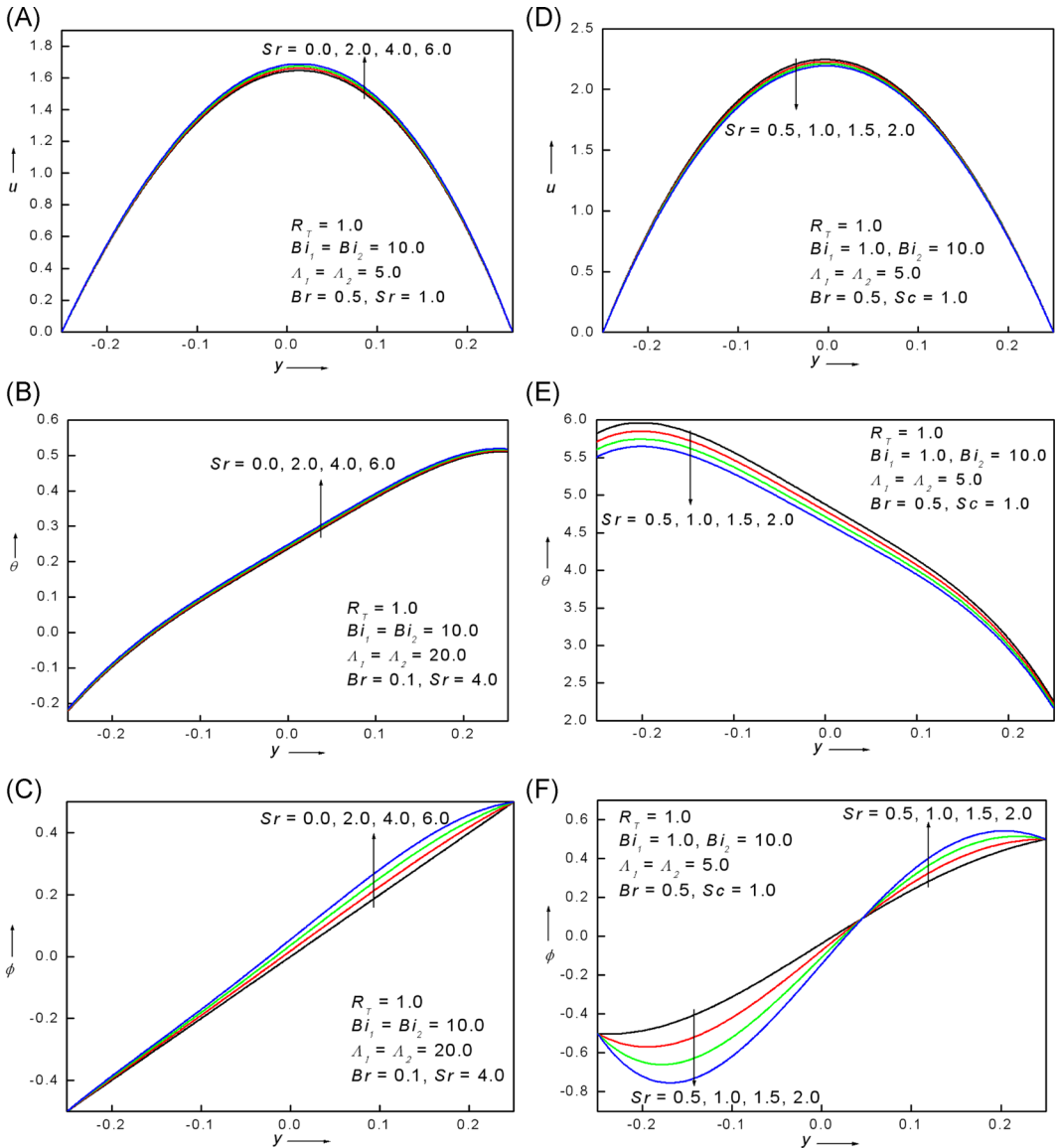
FIGURE 7 A, Velocity profiles for $Sr = 0, 2, 4, 6$. B, Temperature profiles for $Sr = 0, 2, 4, 6$. C, Concentration profiles for $Sr = 0, 2, 4, 6$. D, Velocity profiles for $Sr = 0.5, 1.0, 1.5, 2.0$. E, Temperature profiles for $Sr = 0.5, 1.0, 1.5, 2.0$. F, Concentration profiles for $Sr = 0.5, 1.0, 1.5, 2.0$ [Color figure can be viewed at wileyonlinelibrary.com]

5 | RESULTS AND DISCUSSION

In this part, the results on the buoyancy force and viscous dissipation containing pure viscous fluid for combined effects of the heat and mass transfer within the channel are discussed. The Robin boundary conditions are used for the mixed convection flow. The impacts of major parameters such as thermal Grashof number, mass Grashof number, Schmidt number, Soret number, Brinkman number, symmetric and asymmetric wall temperatures on the heat and mass flow for equal and unequal Biot numbers are analyzed numerically and shown graphically. The equations describing the liquid flow and energy transport are nonlinear and
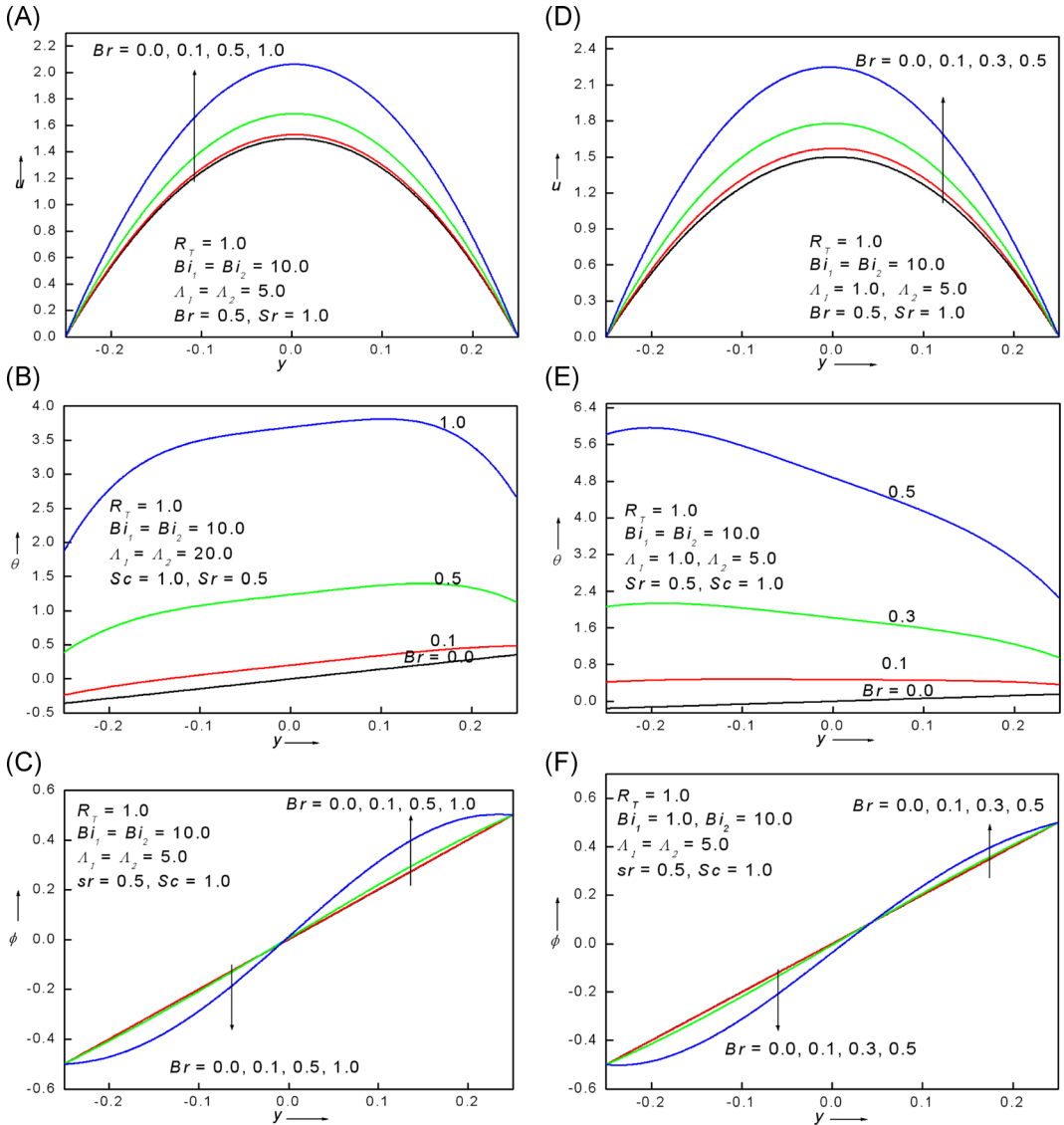
FIGURE 8 A, Velocity profiles for $Br = 0, 0.1, 0.5, 1.0$. B, Temperature profiles for $Br = 0, 0.1, 0.5, 1.0$. C, Concentration profiles for $Br = 0, 0.1, 0.5, 1.0$. D, Velocity profiles for $Br = 0, 0.1, 0.3, 0.5$. E, Temperature profiles for $Br = 0, 0.1, 0.3, 0.5$. F, Concentration profiles for $Br = 0, 0.1, 0.3, 0.5$ [Color figure can be viewed at wileyonlinelibrary.com]

hence the closed form solutions are not possible to find. Hence approximate systematic solutions are obtained using perturbation parameter as Brinkman number Br, but for higher values of Brinkman number, such a solution cannot be applied. To relax this condition on Brinkman number, the numerical results using Runge–Kutta method with shooting technique were obtained. Comparing the solutions which were obtained by perturbation method and Runge–Kutta method with shooting algorithm is valid.

For the negligible viscous dissipation and buoyancy forces, the exact solutions obtained. Heat is transferred by pure conduction at $Br = 0$ with ($R_T = 1$) and temperature is uniform. As shown in Figure 2, the velocity at $\Lambda_1 = 500, 1000$ at cold wall flow is reversal for upward flow Λ_1, and it indicates that at the cold wall, flow reversal occurs by buoyancy forces. At y-axis with $\Lambda_1 = -500, -1000$, it shows that at hot wall the reversal flows are obtained.

In the absence of thermal Grashof number, for different values of Br, the values of the temperature field θ are obtained and are depicted in Figure 3A and 3B for $Bi_1 = Bi_2$ and for $Bi_1 \neq Bi_2$. Since the negligible buoyancy force results in a purely forced convection, therefore, the plots for the field is linear and there is no dissipation ($Br = 0$) for $Bi_1 = Bi_2$ and for $Bi_1 \neq Bi_2$ as represented in Figure 3A and 3B. As the Brinkman number increases, temperature increases for both $Bi_1 = Bi_2$ and for $Bi_1 \neq Bi_2$. However, there is a distinction of profiles for equal and unequal Biot numbers. This is due to the fact that when $Bi_1 = Bi_2 = 10$, one obtains $S = 0.61$ and for $Bi_1 = 1$, $Bi_2 = 10$ the values of $S = 0.25$. That is to say that for unequal Biot numbers, $T(-L/2) > T(L/2)$ and hence the temperature field is very influenced at the cold wall for unequal Biot number.
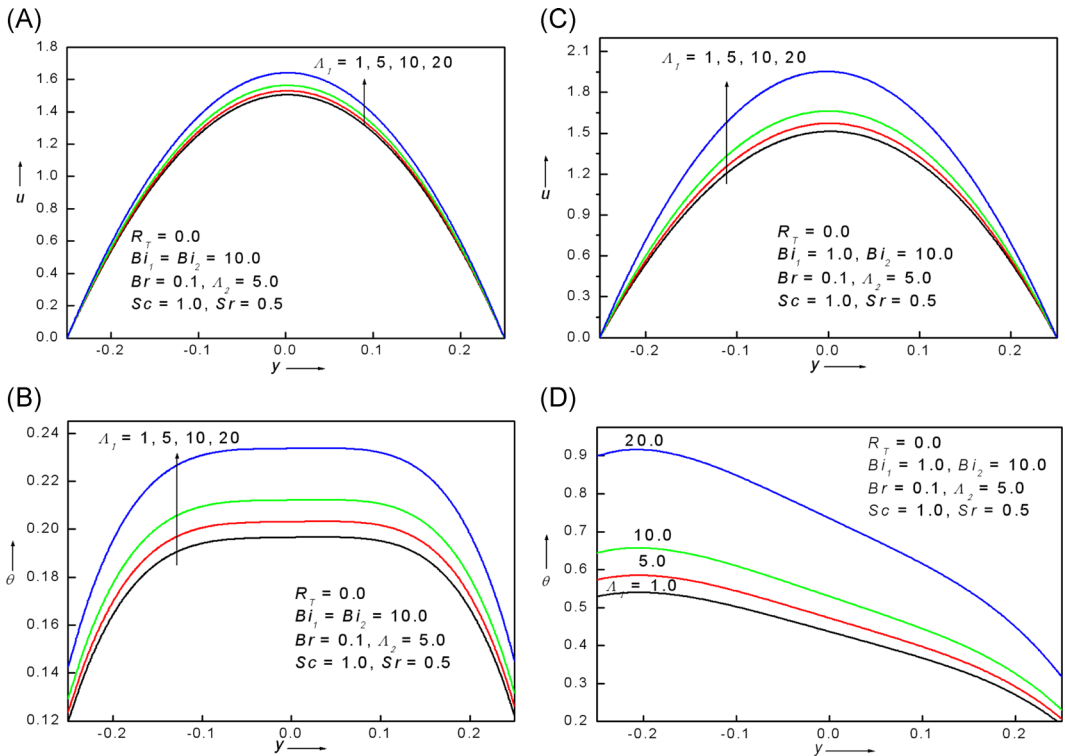
FIGURE 9 A, Velocity profiles for $\Lambda_1 = 1, 5, 10, 20$ with $R_T = 0$. B, Temperature profiles for $\Lambda_1 = 1, 5, 10, 20$ with $R_T = 0$. C, Velocity profiles for $\Lambda_1 = 1, 5, 10, 20$ with $R_T = 0$. D, Temperature profiles for $\Lambda_1 = 1, 5, 10, 20$ with $R_T = 0$ [Color figure can be viewed at wileyonlinelibrary.com]

For asymmetric wall heating condition, the effects of thermal Grashof number Λ_1 (Figure 4A-D) and mass Grashof number Λ_2 (Figure 5A-D) on the velocity field and temperature field for both $Bi_1 = Bi_2$ and for $Bi_1 \neq Bi_2$ are displayed. If the thermal Grashof number Λ_1 increases, both the velocity and temperature fields are enhanced for both $Bi_1 = Bi_2$ and $Bi_1 \neq Bi_2$ as seen in Figure 4A–D. The thermal Grashof number Λ_1 acts as the driving force in the balance equation which results in the increase in the velocity field or velocity gradient. If the effects of viscous dissipation increase, it increases the temperature field. Here also the temperature profiles for $Bi_1 \neq Bi_2$ show significant role at the cold wall as $T(-L/2) > T(L/2)$. As the mass Grashof number Λ_2 increases, the velocity and temperature fields decrease at the cold wall and increase at the hot wall for both cases $Bi_1 = Bi_2$ and $Bi_1 \neq Bi_2$. Also the mass Grashof number effect is not very significant on the flow profiles. However, for $Bi_1 \neq Bi_2$ the effect of mass Grashof number is noticeable at left wall distinctly.

Figure 6A–F illustrate the response of velocity, temperature, and concentration profiles for equal and unequal Biot numbers to different values of Schmidt number Sc. The Schmidt number is a fundamental parameter in species diffusion (mass transfer), which is defined as $Sc = \upsilon/D_m$; therefore on the velocity, temperature, and concentration field, Schmidt effect is more relevant for mass and momentum. When $Sc > 1$, it shows that momentum diffusion rate dominates to the rate of species diffusion, the opposite applies for $Sc < 1$ and for $Sc = 1$, both the rates are as momentum and concentration diffusivity equal. It is observed from Figure 6A–C that as the Schmidt number increases, the velocity, temperature, and concentration increase
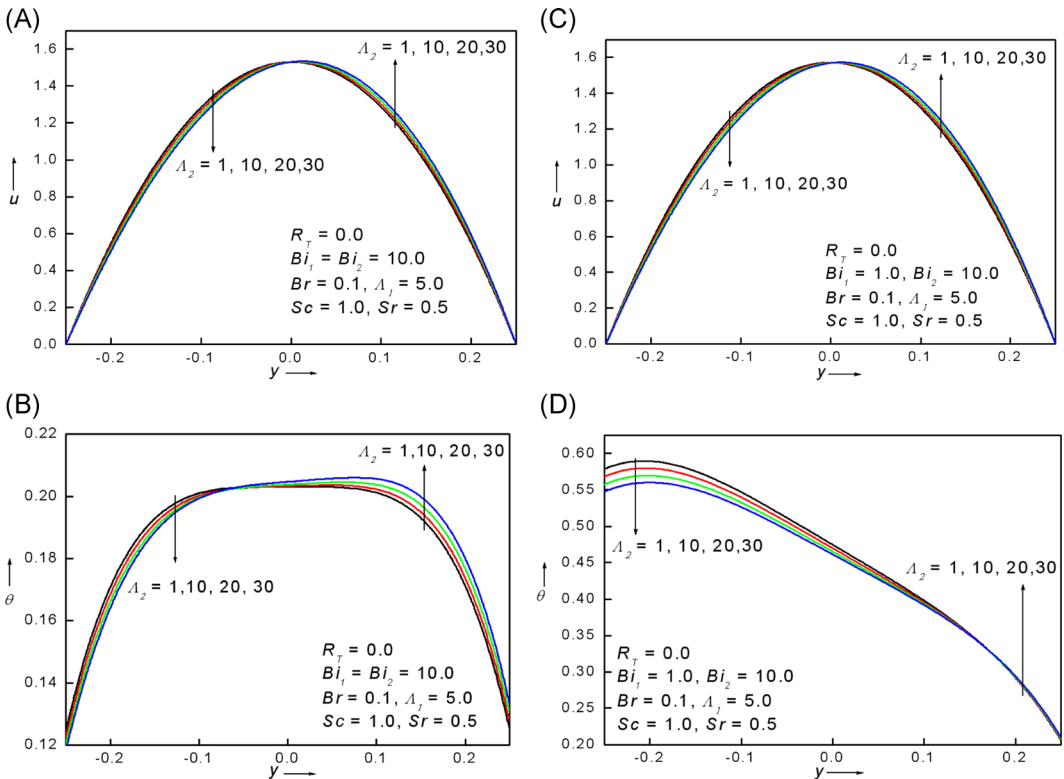

FIGURE 10 A, Velocity profiles for $\Lambda_2 = 1$, 10, 20, 30 with $R_T = 0$. B, Temperature profiles for $\Lambda_2 = 1$, 10, 20, 30 with $R_T = 0$. C, Velocity profiles for $\Lambda_2 = 1$, 10, 20, 30 with $R_T = 0$. D, Temperature profiles for $\Lambda_2 = 1$, 20, 30 with $R_T = 0$ [Color figure can be viewed at wileyonlinelibrary.com]

and its effect is dominant in the center of the channel. Therefore, the mass transfer exerts interplay with the flow field and the distribution of species in material can control via the Schmidt number. The results are similar to the results obtained by Shamshuddin et al[47] who have studied heat and mass transfer for micropolar fluid. However it is interesting to note that when the temperature at the cold wall exceeds the temperature at the hot wall, reversal effect is observed on the flow structure as seen in Figure 6D-F. That is to say that if the Schmidt number increases, then the velocity and temperature fields are suppressed. The concentration field decreases at the left plate from $y = -0.25$ to 0.03 and increases from $y = 0.03$ to 0.25. Hence one can conclude that momentum and concentration diffusivity rates are not only the factors, which account for the velocity, temperature, and mass transport but also the wall heating conditions significantly affect the flow field and the distribution of species within materials.

Figure 7A–F presents the effect of thermodiffusive parameters, that is, Soret number on the velocity, temperature, and concentration fields for both cases, namely, $Bi_1 = Bi_2$ and $Bi_1 \neq Bi_2$. The small light and large heavy molecules are separated under temperature gradient when the effect of Soret arises. This type of effect is most important, where very large temperature gradient in form of more than one chemical species is present. This type of flow can be obtained in polymer material possessing, chemical reactors, and energy generators. The effects of both Soret number Sr and Schmidt number Sc on the flow field for $Bi_1 = Bi_2$ and $Bi_1 \neq Bi_2$ are similar.

TABLE 1 Velocity values for $Br = 0$, 0.01, 0.5, $Sr = 0.5$, $Sc = 1.0$, $\Lambda_1 = 5$, $\Lambda_2 = 5$, and $R_T = 1$ with the series expansion is up to two terms only

	$Bi_1 = Bi_2 = 10$					
	$u = u_0 + Br\, u_1$					
	$Br = 0.0$		$Br = 0.01$		$Br = 0.5$	
y	Analytical	Numerical	Analytical	Numerical	Analytical	Numerical
−0.25	0.00000000	0.00000000	0.00000000	0.00000000	0.00000000	0.00000000
−0.15	0.94285714	0.94285714	0.94439116	0.94474602	1.01955790	1.06153101
−0.05	1.43142857	1.43142857	1.43375111	1.43430160	1.54755535	1.61234542
0.05	1.44857143	1.44857143	1.45089839	1.45144941	1.56491971	1.63032498
0.15	0.97714286	0.97714286	0.97868607	0.97904227	1.05430378	1.09736718
0.25	0.00000000	0.00000000	0.00000000	0.00000000	0.00000000	0.00000000
	$Bi_1 = 1.0, Bi_2 = 10$					
	$u = u_0 + Bru_1$					
	$Br = 0.0$		$Br = 0.01$		$Br = 0.5$	
y	Analytical	Numerical	Analytical	Numerical	Analytical	Numerical
−0.25	0.00000000	0.00000000	0.00000000	0.00000000	0.00000000	0.00000000
−0.15	0.94687500	0.94687500	0.95107542	0.95145802	1.15689620	1.45926542
−0.05	1.43343750	1.43343750	1.43942533	1.44001411	1.73282895	2.16913498
0.05	1.44656250	1.44656250	1.45222051	1.45280675	1.72946301	2.14641314
0.15	0.97312500	0.97312500	0.97666605	0.97704372	1.15017745	1.41288117
0.25	0.000000000	0.000000000	0.00000000	0.00000000	0.00000000	0.00000000

TABLE 2 Velocity values for $Br = 0$, 0.01, 0.5, $Sr = 0.5$, $Sc = 1.0$, $\Lambda_1 = 5$, $\Lambda_2 = 5$, and $R_T = 1$ with 13 terms of the series expansion

	$Bi_1 = Bi_2 = 10$					
	$u = u_0 + Br\ u_1 + Br^2u_2 + Br^3u_3 + Br^4u_4 + Br^5u_5 + Br^6u_6+$					
	$Br^7u_7 + Br^8u_8 + Br^9u_9 + Br^{10}u_{10} + Br^{11}u_{11} + Br^{12}u_{12}$					
	$Br = 0.0$		$Br = 0.01$		$Br = 0.5$	
y	Analytical	Numerical	Analytical	Numerical	Analytical	Numerical
−0.25	0.00000000	0.00000000	0.00000000	0.00000000	0.00000000	0.00000000
−0.15	0.94285714	0.94285714	0.94099251	0.94474602	0.86417250	1.06153101
−0.05	1.43142857	1.43142857	1.42859372	1.43430160	1.31179292	1.61234542
0.05	1.44857143	1.44857143	1.44573261	1.45144941	1.32875501	1.63032498
0.15	0.97714286	0.97714286	0.97526971	0.97904227	0.89807094	1.09736718
0.25	0.000000000	0.00000000	0.00000000	0.00000000	0.00000000	0.00000000
	$Bi_1 = 1.0, Bi_2 = 10$					
	$Br = 0.0$		$Br = 0.01$		$Br = 0.5$	
y	Analytical	Numerical	Analytical	Numerical	Analytical	Numerical
−0.25	0.00000000	0.00000000	0.00000000	0.00000000	0.00000000	0.00000000
−0.15	0.94687500	0.94687500	0.94501037	0.95145802	0.86819041	1.45926542
−0.05	1.43343750	1.43343750	1.43060265	1.44001411	1.31380192	2.16913498
0.05	1.44656250	1.44656250	1.44372368	1.45280675	1.32674615	2.14641314
0.15	0.97312500	0.97312500	0.97125185	0.97704372	0.89405313	1.41288117
0.25	0.00000000	0.00000000	0.00000000	0.00000000	0.00000000	0.00000000

TABLE 3 Velocity and temperature values for $Br = 0.0001$, $Sr = 0.0$, $Sc = 0.0$, $\Lambda_1 = 100$, $\Lambda_2 = 0$, and $R_T = 1$ in comparison with data of Zanchini[41]

	$Bi_1 = Bi_2 = 10$			
	$u = u_0 + Br\ u_1 + Br^2u_2 + Br^3u_3 + Br^4u_4 + Br^5u_5 + Br^6u_6+$			
	$Br^7u_7 + Br^8u_8 + Br^9u_9 + Br^{10}u_{10} + Br^{11}u_{11} + Br^{12}u_{12}$			
	Velocity		Temperature	
	Zanchini	Present model	Zanchini	Present model
y	Analytical	Numerical	Analytical	Numerical
−0.25	0.00000000	0.00000000	−0.35714178	−0.35703534
−0.15	0.81712412	0.81752467	−0.21429491	−0.21410690
−0.05	1.36854296	1.36916041	−0.07143830	−0.07122816
0.05	1.51140007	1.51202552	0.07141881	0.07163487
0.15	1.10283833	1.10325603	0.21427638	0.21449135
0.25	0.00000000	0.00000000	0.35713677	0.35728440

TABLE 4 Values of Nusselt number, mean velocity, and bulk temperature with $\Lambda_1 = \Lambda_2 = 5.0$, $R_T = 1.0$, $Br = 0.1$, $Sc = 1.0$, $Sr = 0.5$

	$Bi_1 = Bi_2 = 10$				$Bi_1 = 1.0, Bi_2 = 10$			
	Nu_1	Nu_2	$\bar{u}$	θ_b	Nu_1	Nu_2	$\bar{u}$	θ_b
Λ_1								
0	3.6515	0.3021	1.2464	0.15178	−59.2228	64.9470	1.2464	0.33778
10	3.6121	0.2755	1.2858	0.15447	−72.0313	79.4484	1.3342	0.34228
15	3.5929	0.2619	1.3055	0.15581	−80.7047	89.2757	1.3779	0.34426
20	3.5743	0.2480	1.3252	0.15716	−91.6998	101.739	1.4214	0.34608
Λ_2								
0	3.6595	0.3072	1.2696	0.15216	−49.4660	53.9146	1.2942	0.34218
10	3.6044	0.2701	1.2625	0.15415	−94.2616	104.644	1.2866	0.33822
15	3.5780	0.2508	1.2590	0.15526	−169.428	189.928	1.2828	0.33647
20	3.5524	0.2311	1.2554	0.15644	−790.786	895.445	1.2790	0.33485
Br								
0	2.0000	2.0000	1.2500	0.00170	2.0000	2.00000	1.2500	0.00057
0.01	2.164	1.82801	1.2661	0.15312	2.42166	1.56269	1.2904	0.34013
0.5	9.9766	−6.3665	1.3304	0.76782	−2.40419	6.56769	1.4519	1.74674
1.0	17.522	−14.278	1.4108	1.55419	−1.94364	6.09004	1.6537	3.58733

To know the effects of viscous dissipation on the flow, the Brinkman number is varied and the results are displayed graphically in Figure 8A–F for the concentration and flow fields for both $Bi_1 = Bi_2$ and $Bi_1 \neq Bi_2$. As the Brinkman number increases, then velocity and temperature fields are promoted. This result is very casual because when Brinkman number Br increases, then both fields, namely, temperature and velocity, also increase for two considered cases for the Biot numbers. However, the effect of Brinkman number at the cold wall is highly significant compared to the hot wall for the case of $T(-L/2) > T(L/2)$. For equal Biot numbers, Figure 8C shows that as Br increases, the concentration decreases from $y = -0.25$ to 0.0 and then increases from $y = 0.0$ to 0.25. For unequal Biot numbers, the concentration decreases from $y = -0.25$ to 0.02, whereas it increases from $y = 0.02$ to 0.25 as depicted in Figure 8F. The concentration reversal point is varied for both cases as $Bi_1 = Bi_2$ and $Bi_1 \neq Bi_2$ as there will be change in wall temperatures.

As shown in Figures 2 to 8, the graphs are drawn for asymmetric wall heating condition ($R_T = 1$). The results are drawn for symmetric wall temperatures in Figures 9 and 10 for the variations of thermal Grashof number Λ_1 and mass Grashof number Λ_2 for $Bi_1 = Bi_2$ and $Bi_1 \neq Bi_2$. The results are similar to asymmetric wall heating conditions as seen in Figures 4 and 5. This implies that, as the thermal Grashof number increases then the velocity and temperature fields are enhanced for both equal (Figure 9A and 9B) and unequal (Figure 9C and 9D) Biot numbers. Here, also the temperature field is dominated at the left wall compared to the right wall when the thermal Grashof number affects on the temperature field for unequal Biot number. The effect of mass Grashof number is to suppress the velocity and temperature fields at the left wall and promote at the right wall for equal Biot number as predicted in Figure 10A and 10B. For $Bi_1 \neq Bi_2$, velocity increases at the hot wall and reduces at the cold wall, whereas it decreases the temperature field at the left wall and no effect is observed at the right wall as seen in Figure 10C and 10D, respectively.

For justification purpose, we compared the analytical and numerical solutions by using Tables 1 and 2. In Table 1, the series of two terms is found for analytical solutions as u (ie, $u = u_0 + Br \cdot u_1$) for $Bi_1 = Bi_2$ and $Bi_1 \neq Bi_2$. Comparing these analytical and numerical results, we can conclude that when $Br = 0$, both solutions are equal. At $Br = 0.01$, up to two decimal places, both the solutions are

equal for both $Bi_1 = Bi_2$ and $Bi_1 \neq Bi_2$, and for $Br = 0.5$, it is seen that the both analytical and numerical solutions are not equal with small error in the considered cases for the Biot numbers. Similarly, for the series expansion of u up to 13 terms, the analytical and numerical solutions are equal for $Br = 0$. Analytical and numerical solutions agree up to two decimal places when $Br = 0.01$ at $Bi_1 = Bi_2$ and $Bi_1 \neq Bi_2$. When $Br = 0.5$ it is observed that the maximum error occurs between the analytical and numerical solutions for both $Bi_1 = Bi_2$ and $Bi_1 \neq Bi_2$. However one can observe from Tables 1 and 2, that we can minimize this error by considering thirteen terms of the series instead of two terms in numerical and analytical solution. Here we do not compare the values of temperature field. It follows only for velocity field. For further observation of the numerical solutions, the present problem is solved in the absence of the chemical reaction and as shown in results with Zanchini[46] by considering large series expansion as for thirteen terms and it is tabulated in Table 3. From this, we observed that the numerical solutions of the present model agree with Zanchini.[46]

In Table 4, we tabulated the effects of thermal Grashof number Λ_1, mass Grashof number Λ_2, and Brinkman number Br on the Nusselt number Nu, mean velocity $\bar{u}$, and on bulk temperature θ_b. Increase in the thermal Grashof number decreases the Nusselt number at the left and right walls but the values of average velocity $\bar{u}$ and bulk temperature θ_b are increased with raising the thermal Grashof number for $Bi_1 = Bi_2$. For the case of $Bi_1 \neq Bi_2$, the Nusselt number decreases at the cold wall and the Nusselt number increases at the hot wall, whereas the average velocity $\bar{u}$ and bulk temperature θ_b are increased with the thermal Grashof number. Increasing the value

TABLE 5 Values of skin friction with $\Lambda_1 = \Lambda_2 = 5.0$, $R_T = 1.0$, $Br = 0.1$, $Sc = 1.0$, $Sr = 0.5$

	$Bi_1 = Bi_2 = 10$		$Bi_1 = 1.0, Bi_2 = 10$	
	τ_1	τ_2	τ_1	τ_2
Λ_1				
0	11.7542	−12.1708	11.7542	−12.1708
10	11.9041	−12.9218	12.7921	−13.1961
15	11.9782	−13.2991	13.3074	−13.7076
20	12.0521	−13.6778	13.8203	−14.2183
Λ_2				
0	12.0758	−12.3743	12.5242	−12.5146
10	11.5834	−12.7170	12.0248	−12.8531
15	11.3373	−12.8882	11.7755	−13.0223
20	11.0913	−13.0591	11.5264	−13.1914
Br				
0	11.6429	−12.3571	11.7266	−12.2734
0.1	11.8295	−12.5457	12.2744	−12.6838
0.5	12.5761	−13.2999	14.4656	−14.3256
1.0	13.5093	−14.2427	17.2046	−16.3778
Sr				
0.5	11.8295	−12.5457	12.2744	−12.6839
1.0	11.7921	−12.5081	12.2369	−12.6463
1.5	11.7547	−12.4704	12.1995	−12.6087
2.0	11.7173	−12.4328	12.1621	−12.5711
Sc				
0.5	11.8482	−12.5645	12.2931	−127027
1.0	11.8295	−12.5457	12.2744	−12.6838
1.5	11.8108	−12.5269	12.2557	−12.6651
2.0	11.7921	−12.5081	12.2369	−12.6463

TABLE 6 Values of Sherwood numbers with $\Lambda_1 = \Lambda_2 = 5.0$, $R_T = 1.0$, $Br = 0.1$, $Sc = 1.0$, $Sr = 0.5$

	$Bi_1 = Bi_2 = 10$		$Bi_1 = 1.0, Bi_2 = 10$	
	Sh_1	Sh_2	Sh_1	Sh_2
Sr				
0.5	1.41397	2.61461	1.41041	2.61078
1.0	0.82793	3.22921	0.82150	3.22225
1.5	0.24324	3.84515	0.23327	3.83445
2.0	−0.34056	4.46199	−0.35426	4.44723
Sc				
0.5	1.70665	2.30697	1.70512	2.30531
1.0	1.41352	2.61416	1.41041	2.61078
1.5	1.12062	2.92157	1.11587	2.91643
2.0	0.82793	3.22921	0.82150	3.22225
Br				
0	2.00000	2.00000	2.00000	2.00000
0.1	1.41397	2.61460	1.41075	2.61112
0.5	−0.93017	5.07302	−0.94625	5.05562
1.0	−3.86033	8.14605	−3.89249	8.11124

of mass Grashof number, the Nusselt number at both the walls and velocity $\bar{u}$ are decreased, whereas the bulk temperature θ_b increases. For $Bi_1 \neq Bi_2$, increasing the values of mass Grashof number decreases the Nusselt number at left wall and increases at the right wall, whereas the velocity $\bar{u}$ and bulk temperature θ_b are decreased. Increasing the Brinkman number Br, the Nusselt number increases at the left wall, whereas it decreases at the right wall, whereas the mean velocity and bulk temperature are increased for $Bi_1 = Bi_2$. While for the case of $Bi_1 \neq Bi_2$, the Nusselt number decreases at the left wall and increases at the right wall but the mean velocity and bulk temperature are increased as the Brinkman number increases.

Then in Table 5, we observed the effects of thermal Grashof number, mass Grashof number, Brinkman number, Soret number, and Schmidt number on the skin friction. Increasing the values of thermal Grashof number increases the values of skin friction at left wall and decreases the value at right wall for $Bi_1 = Bi_2$ and $Bi_1 \neq Bi_2$. The rise of the mass Grashof number decreases the skin friction at both the walls for two considered case for the Biot numbers. Increasing the value of Brinkman number, the values of skin friction are also increased at the left wall and decreased at the right wall for both Biot numbers cases. The values of skin friction are decreased at the left wall and increased at the right wall for increasing values of Soret and Schmidt numbers for both Biot numbers cases.

The effects of the Brinkman number, Soret number, and Schmidt number on the Sherwood number Sh for $Bi_1 = Bi_2$ and $Bi_1 \neq Bi_2$ are shown in Table 6. Increasing the values of Soret, Schmidt, and Brinkman numbers the values of Sherwood number are decreased at the cold wall and Sherwood numbers are increased at the hot wall for both Biot numbers cases.

6 | CONCLUSIONS

Results are obtained with combined effects of buoyancy force and viscous dissipation containing pure viscous fluid. The thermal boundary conditions of third kind are used for the mixed convection flow and results are obtained for different Biot numbers with symmetric and asymmetric wall temperatures. For small values of the perturbation parameter (Brinkman

number), we obtained the results by analytical method, and for large values of this parameter, we got the results using numerical technique based on the Runge–Kutta fourth-order algorithm with shooting approach. The thermal Grashof number, mass Grashof number, Schmidt number, Soret number, Brinkman number, and symmetric and asymmetric wall temperatures enhance the flow and energy transport. The concentration field was suppressed at the left wall and promoted at the right wall for the effects of Schmidt number, Soret number, and Brinkman number for both equal and unequal Biot numbers. If there is no Brinkman number, then the solutions found analytically and numerically were exact and little variation can be found when the Brinkman number increases. The numerical and analytical solutions are similar to Zanchini data[46] in the absence of Schmidt number and Soret number.

NOMENCLATURE

A	constant (Pa/m)
Bi_1, Bi_2	Biot numbers
Br	Brinkman number
Sr	Soret number
Sc	Schmidt number
C_p	specific heat at constant pressure
C_1, C_2	reference concentration of the external fluid
C_0	reference concentration
C	concentration
$D\ (=2L)$	hydraulic diameter (m)
D_m	mass diffusivity of the solute
g	acceleration due to gravity (m/s)
Gr_T	Grashof number ($g\beta\Delta TD^3/v^2$)
Gr_C	solute Grashof number ($g\beta\Delta CD^3/v^2$)
h_1, h_2	external heat transfer coefficients (W·m^{-2}·k^{-1})
k	thermal conductivity (W·m^{-1}·k^{-1})
L	channel width (m)
n	non-negative integer number
Nu_1, Nu_2	Nusselt numbers
p	pressure (Pa)
$P = p + \rho_0 gX$	difference between the pressure and the hydrostatic pressure (Pa)
Pr	Prandtl number (v/α)
Re	Reynolds number ($U_0 D/v$)
Sh_1, Sh_2	Sherwood numbers
R_T	temperature difference ratio (($T_2 - T_1)/\Delta T$)
S	dimensionless parameter
T	temperature (K)
T_1, T_2	reference temperature of the external fluid (K)
T_0	reference temperature (K)
u	dimensionless velocity in the X-direction
$u_n\left(y\right)$	dimensionless functions
$\bar{u}$	mean value of u
U	velocity component in the X-direction (m/s)
X	stream wise co-ordinate (m)

y	dimensionless transverse co-ordinate
Y	transverse co-ordinate (m)

GREEK SYMBOLS

α	thermal diffusivity ($K/\rho_0 c_0$) (m^2/s)
β_T	thermal expansion coefficient (K^{-1})
β_C	concentration expansion coefficient
ΔT	reference temperature
ΔC	reference concentration
τ_1, τ_2	skin frictions
ε	dimensionless parameter
θ	dimensionless temperature
θ_b	dimensionless bulk temperature
ϕ	dimensionless concentration
μ	dynamic viscosity (Pa/s)
ν	kinematic viscosity (μ/ρ_0) (m^2/s)
Λ_1	thermal Grashof number (Gr_T/Re)
Λ_2	mass Grashof number (Gr_C/Re)
ρ	mass density (kg/m^3)
ρ_0	value of the mass density when $T = T_0$ (kg/m^3)

ORCID

Mikhail A. Sheremet http://orcid.org/0000-0002-4750-0227

REFERENCES

1. Tao TN. On combined free and forced convection in channels. *J Heat Transfer.* 1960;82:233-238.
2. Aung W, Worku G. Theory of fully developed combined convection including flow reversal. *J Heat Transfer.* 1986;108:485-488.
3. Aung W, Worku G. Developing flow and flow reversal in a vertical channel with asymmetric wall temperature. *J Heat Transfer.* 1986;108:299-304.
4. Barletta A. Fully developed mixed convection and flow reversal in a vertical rectangular duct with uniform wall heat flux. *Int J Heat Mass Transfer.* 2002;45:641-654.
5. Umavathi JC, Patil MB, Pop I. On laminar mixed convection flow in a vertical porous stratum with symmetric wall heating conditions. *Int J Trans Phenom.* 2006;8:127-140.
6. Kumar JP, Umavathi JC, Pop I, Biradar BB. Fully developed mixed convection flow in a vertical channel containing porous and fluid layers with isothermal or isoflux boundaries. *Transp Porous Media.* 2009;80:117-135.
7. Kumar JP, Umavathi JC, Biradar BM. Mixed convection of composite porous medium in a vertical channel with asymmetric wall heating conditions. *J Porous Media.* 2010;13:271-285.
8. Kumar JP, Umavathi JC, Biradar BM. Mixed convection of magneto hydrodynamic and viscous fluid in a vertical channel. *Int J Non-Linear Mech.* 2011;46:278-285.
9. Kumar JP, Umavathi JC, Biradar BM. Mixed convective flow of immiscible viscous fluids in a vertical channel. *Heat Transfer–Asian Res.* 2011;40:1-25.
10. Das UN, Deka RK, Soundalgekar VM. Effects of mass transfer on flow past an impulsively started infinite vertical plate with constant heat flux and chemical reaction. *Forschung im Ingenieurwesen Eng Res.* 1994;60:284-287.
11. Muthucumarswamy R, Ganesan P. First order chemical reaction on flow past an impulsively started vertical plate with uniform heat and mass flux. *Acta Mech.* 2001;147:45-57.

12. Kumar JP, Umavathi JC, Kalyan S. Free convective flow of electrically and viscous immiscible fluid flow in a vertical channel in the presence of first-order chemical reaction. *Heat Transfer–Asian Res.* 2015;44:657-680.

13. Kumar JP, Umavathi JC, Kalyan S. Effect of chemical reaction on mixed convective flow in a vertical channel containing porous and fluid layer. *J Porous Media.* 2017;20:1043-1058.

14. Umavathi JC, Sultana J. Mixed convection flow of a micropolar fluid with concentration in a vertical channel in the presence of heat source or sink. *Int J Math Archive.* 2012;3:3556-3569.

15. Umavathi JC, Mohiuddin S. Mixed convection flow of permeable fluid in a vertical channel in the presence of first-order chemical reaction: variable properties. *Spec Topics Rev Porous Media.* 2018;9:155-176.

16. Li MC, Tian YW, Zhai YC. Soret and Dufour effects in strongly endothermic chemical reaction system of porous media. *Trans Nonferrous Metals Society China.* 2006;16:1200-1204.

17. Sheremet MA. The influence of cross effects on the characteristics of heat and mass transfer in the conditions of conjugate natural convection. *J Eng Thermophys.* 2010;19:119-127.

18. Kandasamy R, Periasamy K, Sivagnanam, Prabhu KK. Chemical reaction, heat and mass transfer on MHD flow over a vertical Stretching Surface with Heat Source and Thermal Stratification Effects. *Int J Heat Mass Transfer.* 2005;48:4557-4561.

19. Kandasamy R, Periasamy K, Sivagnana, Prabhu KK. Effect of chemical reaction, heat and mass transfer along a wedge with heat source and concentration in the presence of suction or injection. *Int J Heat Mass Transfer.* 2005;48:1388-1394.

20. Seddeek MA. Thermal radiation and buoyancy effects on MHD free convection heat generation flow over an accelerating permeable surface with temperature dependent viscosity. *Can J Phys.* 2001;79:725-732.

21. Seddeek MA, Darwish AA, Abdelmeguid MS. Effect of chemical reaction and variable viscosity on hydromagnetic mixed convection heat and mass transfer for Hiemenz flow through porous media with radiation. *Commun Nonlinear Sci Numer Simul.* 2007;12:195-213.

22. Seddeek MA, Salem AM. The effect of an axial magnetic field on the flow and heat transfer about a fluid underlying the axisymmetric spreading surface with temperature dependent viscosity and thermal diffusivity. *Comput Mech.* 2007;39:401-408.

23. Seddeek MA, Faiza AS. The effects of temperature dependent viscosity and thermal conductivity on unsteady MHD convective heat transfer past a semi-infinite vertical porous moving plate with variable suction. *Comput Mater Sci.* 2007;40:186-192.

24. Chamkha AJ, Ben-Nakhi A. MHD mixed convection-radiation interaction along a permeable surface immersed in a porous medium in the presence of Soret and Dufour's effect. *Heat Mass Transfer.* 2008;44:845-856.

25. Pal D, Mondal H. Effects of Soret Dufour, chemical reaction and thermal radiation on MHD non-Darcy unsteady mixed convective heat and mass transfer over a stretching sheet. *Commun Nonlinear Sci Numer Simul.* 2011;16:1942-1958.

26. Shivaiah S, Rao A. Soret and Dufour effects on transient MHD flow past a semi infinite vertical porous plate with chemical reaction. *J Nav Archit Marine Eng.* 2011;8:37-48.

27. Zheng LC, Jin X, Zhang XX, Zhang JH. Unsteady heat and mass transfer in MHD flow over an oscillatory stretching surface with Soret and Dufour effects. *Acta Mechanica Sinica.* 2013;29:667-675.

28. Cheng CY. Soret and Dufour effects on mixed convection heat and mass transfer from a vertical wedge in a porous medium with constant wall temperature and concentration. *Transp Porous Media.* 2012;94:123-132.

29. Devi SPA, Devi RU. Soret and Dufour effects on MHD slip flow with thermal radiation over a porous rotating infinite disk. *Commun Nonlinear Sci Numer Simul.* 2011;16:1917-1930.

30. Rashad A, Chamkha AJ. Heat and mass transfer by natural convection flow about a truncated cone in porous media with Soret and Dufour effects. *Int J Numer Methods Heat Fluid Flow.* 2014;24:595-612.

31. Shivaiah S, Rao JA. Effects of Soret Dufour and thermal radiation on unsteady MHD free convection flow past an infinite vertical porous plate in the presence of chemical reaction. *Int J Appl Math Mech.* 2011;7:58-76.

32. Makinde OD. On MHD mixed convection with Soret and Dufour effects past a vertical plate embedded in a porous medium. *Lat Am Appl Res.* 2011;41:63-68.

33. Rashidi MM, Rahimzadeh N, Ferdows M, Jashim Uddin Md, Anwar Beg O. Group theory and differential transform analysis of mixed convective heat and mass transfer from a horizontal surface with chemical reaction effects. *Chem Eng Commun.* 2012;199:1012-1043.

34. Sarwar S, Rashidi MM. Approximate solution of two-term fractional-order diffusion, wave-diffusion, and telegraph models arising in mathematical physics using optimal homotopy asymptotic method. *Waves Random Complex Media*. 2016:365-382. https://doi.org/10.1080/17455030.2016.1158436

35. Rashidi MM, Siddiqui AM, Asadi M. Application of homotopy analysis method to the unsteady squeezing flow of a second-grade fluid between circular plates. *Math Probl Eng*. 2010;2010:706840.

36. Hasan H, Rashidi MM. An analytic solution of micropolar flow in a porous channel with mass injection using homotopy analysis method. *Int J Num Methods Heat Fluid Flow*. 2014;24:419-437.

37. Rashidi MM, Shooshtari A, Anwar Beg O. Homotopy perturbation study of nonlinear vibration of Von Karman rectangular plates. *Comput Struct*. 2012;106-107:46-55.

38. Makinde OD, Olanrewaju PO. Unsteady mixed convection with Soret and Dufour effects past a porous plate moving through a binary mixture of chemically reacting fluid. *Chem Eng Commun*. 2011;198:920-938.

39. Wibulswas P, Laminar flow heat transfer in non circular ducts, Ph.D. Thesis, London University. 1966. (As reported by Shah and London in 1971).

40. Lyczkowski RW, Solbrig CW, Gidaspow D, Forced convective heat transfer in rectangular ducts-general case of wall resistance and peripheral conduction, Institute of Gas Technology Tech. Info, Center File 3229, 3424S, State, Street, Chicago, I11.60616, 1969 (as reported by Shah and London in 1971).

41. Javeri V. Analysis of laminar thermal entrance region of elliptical and rectangular channels with Kantorowich method. *Warme-und Stoffuberragung*. 1976;9:85-98.

42. Hicken E. Das temperature field in laminar durchstromten Kanalen mitechteckquerschnit beiunterschie-dlicher Beheizung der Kanalwade. *Warme-und Stoffubertragung*. 1968;1:98-104.

43. Sparrow EM, Siegal R. Application of variational methods to the thermal entrance region of ducts. *Int J Heat Mass Transfer*. 1960;1:161-172.

44. Javeri V. Heat transfer in laminar entrance region of a flat channel for the temperature boundary condition of the third kind. *Warme-und Stoffubertragung*. 1977;10:137-144.

45. Javeri V. Laminar heat transfer in a rectangular channel for the temperature boundary condition of the third kind. *Int J Heat Mass Transfer*. 1978;10:1029-1034.

46. Zanchini E. Effect of viscous dissipation on mixed convection in a vertical channel with boundary conditions of the third kind. *Int J Heat Mass Transfer*, 41(1998):3949-3959.

47. Shamshuddin MD, Chamkha AJ, Thumm T, Raju MC. Computation of unsteady MHD mixed convective heat and mass transfer in dissipative reactive micropolar flow considering Soret and Dufour effects. *Front Heat Mass Transfer*. 2018;10:1-15.